Universal scaling of the stress-strain curve in amorphous solids

Jie Lin[1,2,*] and Wen Zheng[3,†]

[1]*Department of Physics, Center for Soft Matter Research, New York University, New York 10003, USA*
[2]*School of Engineering and Applied Sciences, Harvard University, Cambridge, Massachusetts 02138, USA*
[3]*Department of Physics, University of Science and Technology of China, Hefei 230026, People's Republic of China*

The yielding transition of amorphous solids is a phase transition with a special type of universality. Critical exponents and scaling relations have been defined and proposed near the yield stress. We show here that, even in the initial stage of shear far below the yield stress, the stress-strain curve of amorphous solids also shows critical scaling with universal exponents. The key point is to remove the elastic part of the strain, and the shear stress exhibits a sublinear scaling with the plastic strain. We show how this critical scaling is related to the finite size effect of the minimum strain to trigger the first plastic avalanche after a quench. We point out that this sublinear scaling between the stress and the plastic strain implies the divergence of a high-order shear modulus. A scaling relation is derived between two exponents characterizing the stress-strain curve and the density distribution of the local stabilities, respectively. We test the critical scaling of the stress-strain curve using both mesoscopic and atomistic simulations and get satisfying agreement in two and three dimensions.

The stress-strain curve characterizes the response of amorphous solids, such as emulsions, foams, and molecular glasses against the external shear stress [1–4]. In the beginning of shear, the materials respond elastically, and as one increases the stress or strain further, the plastic deformation starts to accumulate. When the stress reaches the yield stress, the stress-strain curve enters a plateau, and the system starts to flow [5–8]. The corresponding transition is called the yielding transition. A lot of attention has been focused on the critical dynamics near the yielding transition [9–12], e.g., power-law distributed avalanches and singular flow curves with a series of critical exponents. On the other hand, much less investigation has been performed on the beginning stage of the stress-strain curve. It is well known that the deviation of the stress-strain curve from the linear behavior is because of the plastic strain, hidden in the stress-strain curve and reflecting the amount of elastic energy that has been relaxed by plasticity. A common protocol to investigate the stress-strain curve is to first quench a fluid at high temperatures to zero temperature and apply a quasistatic shear afterwards as illustrated in Fig. 1(a). It has been shown that the minimum strain $\gamma_{\min}$ to trigger the first plastic deformation after a thermal quench exhibits a nontrivial finite size scaling with the system size N, $\gamma_{\min} \sim N^{-1/(1+\theta_0)}$ with the exponent $\theta_0 \approx 0.5$ [13–15]. It is thus natural to ask if there is any other critical behavior hidden in the mechanical response of amorphous solids even at low stress. In this paper, we show that the stress-strain curve indeed exhibits universal scaling behavior at low stress after we subtract the elastic part of the strain.

During the plastic deformation, localized plastic rearrangements, shear transformation zones, organize into avalanches mediated by the long-range elastic coupling [16–20]. Experimentally, one can apply either the strain-control or the stress-control method. In the strain-control case, the stress is relaxed, and the total strain is fixed during plastic avalanches,

whereas in the stress-control case, the stress is fixed, and the total strain increases during plastic avalanches [21]. For both methods, the stress is increased quasistatically between two consecutive avalanches, and the resulting stress-strain curves (σ vs γ) coincide in the thermodynamic limit. The comparisons between the two methods on the microscopic scale are shown in the insets of Figs. 1(b) and 1(c). The avalanches in the stress-control case can be considered to be composed of several avalanches in the strain-control case as illustrated in the inset of Fig. 1(b) in which the plastic stress drop $\delta\sigma_p$ and the plastic strain increment $\delta\epsilon$ also are shown. From the slope of the stress-strain curve in the limit $\gamma \to 0$, we can get the shear modulus $\mu = d\sigma/d\gamma (\gamma \to 0)$ as shown in Fig. 1(b). Because the elastic strain is proportional to the stress by the shear modulus, one can extract the plastic strain as the difference between the total strain and the elastic strain,

$$\epsilon = \gamma - \frac{\sigma}{\mu}, \tag{1}$$

where the second part on the right side is the elastic part of the total strain. The resulting stress-plastic strain curve is shown in Fig. 1(c). The main point of this paper is to show that the scaling relation between the stress and the plastic strain at low stress is singular,

$$\sigma \sim \epsilon^{\alpha}, \tag{2}$$

with $\alpha < 1$ and a scaling relation exists between α and θ_0. Because θ_0 is universal, so is α. Moreover, the above scaling relation between the stress and the plastic strain implies that the high-order shear modulus diverges, consistent with recent calculations in the infinite dimensions [1]. In the following, we first derive the scaling relation between the stress and the plastic strain. Then we explain how θ_0 is connected to α and argue their universality. We prove that a singular relation between the stress and the plastic strain gives rise to the divergence of a high-order shear modulus. Finally, we test our theories using both the mesoscopic elastoplastic model [8,12,22,23] and the atomistic numerical simulations and get

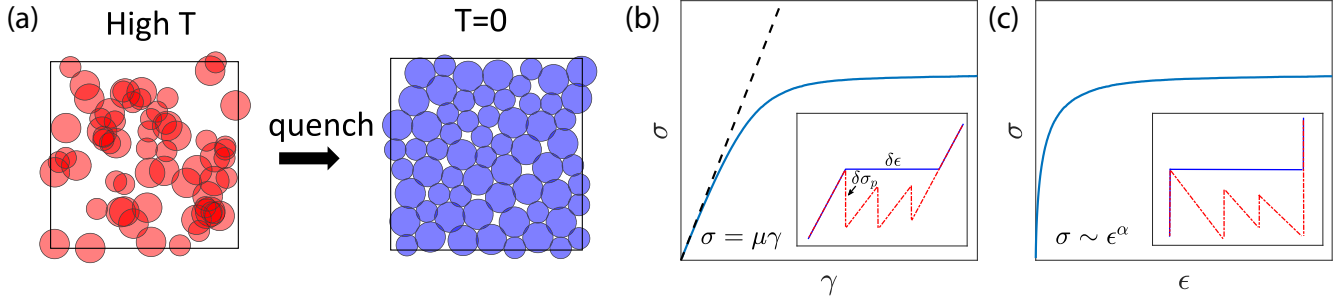*jielin@g.harvard.edu
†wenzheng@ustc.edu.cn

FIG. 1. (a) Before the implementation of shear, one typical way to prepare the amorphous solid is to rapidly quench a fluid at high temperatures to zero temperature. (b) After the quench, one can exert quasistatic shear by the stress-control or strain-control method. The main panel shows the resulting stress- (σ-) strain (γ) curve. The two methods coincide in the thermodynamic limit, and their difference on the microscopic scale is shown in the inset: during the plastic deformation (avalanches), the stress is conserved in the stress-control case (blue) whereas the stress relaxes in the strain-control case (red). The resulting plastic strain increment $\delta\epsilon$ and plastic stress drop $\delta\sigma_p$ are shown. In the limit $\gamma \to 0$ (or $\sigma \to 0$), the slope of the stress-strain curve becomes the shear modulus μ. (c) The stress-plastic strain (ϵ) curve after subtracting the elastic strain part. In the low stress limit, the stress has a power-law scaling relation with the plastic strain. The inset shows the difference between the stress-control and the strain-control methods.

satisfying agreement in both two dimensions (2D) and three dimensions (3D).

I. THEORETICAL DERIVATIONS

Since the stress-strain curves are the same for stress-control and strain-control protocols, we focus on the stress-control case, and the conclusions equally are valid for the strain-control case. Between two plastic avalanches, the stress increment $\delta\sigma$ to trigger the next avalanche during quasistatic shear scales as $\delta\sigma \sim N^{-1/[1+\theta(\sigma)]}$. The θ exponent is a function of σ and varies between 0 and 1 [2,15]. The plastic strain increment [the length of the blue horizontal line in the inset of Fig. 1(c)] due to the triggered avalanche becomes $\delta\epsilon \sim S/N$, where S is the avalanche size, which is the number of local plastic events involved in the avalanche. Given the expressions of $\delta\sigma$ and $\delta\epsilon$, we can find the expression for the local slope of the stress-plastic strain curve in the thermodynamic limit,

$$\frac{\partial\sigma}{\partial\epsilon} \sim \frac{N^{\theta/(\theta+1)}}{\langle S \rangle}. \quad (3)$$

Because the first triggered avalanche only involves a finite number of local plastic events as supported numerically [24], we have $S \sim 1$ as $\epsilon \to 0$ and obtain

$$\partial\sigma/\partial\epsilon \sim N^{\theta_0/(\theta_0+1)}. \quad (4)$$

Here $\theta_0 = \theta(\sigma \to 0)$, the θ exponent right after the quench. On the other hand, because $\epsilon \sim N^{-1}$ in the limit $\epsilon \to 0$, one can write Eq. (4) as $\partial\sigma/\partial\epsilon \sim \epsilon^{-[\theta_0/(\theta_0+1)]}$. After integration, we obtain the scaling relation between the stress and the plastic strain in the initial stage of shear, $\sigma \sim \epsilon^\alpha$ with

$$\alpha = \frac{1}{1+\theta_0}. \quad (5)$$

The θ exponent is also the exponent characterizing the distribution of local stability. In the elastoplastic viewpoint, the amorphous solid is coarse grained into N blocks, each characterized by a local scalar stress σ_i and a local failure threshold σ_i^{th}. The local stability of block i is defined as $x_i = \sigma_i^{\text{th}} - \sigma_i$. It has been shown that the distribution of

the local stabilities scales as $P(x) \sim x^\theta$ for small x [8,25]. To trigger an instability, one only needs to destabilize the least stable block, and the stress increment is essentially the smallest x in a finite system $\delta\sigma \sim x_{\min} \sim N^{-[1/(1+\theta)]}$. The values of the θ exponent have been reported to be universal right after a quench [25,26], $\theta_0 \approx 0.5$ for both two and three dimensions. The mean field value of $\theta_0 = 1/2$ in the infinite dimensions limit has been calculated exactly [20], consistent with simulations in finite dimensions. Given the universal value of θ_0, one obtains

$$\alpha = \frac{2}{3}, \quad (6)$$

which is universally valid as well. Mean field models [20] and numerical simulations [15] have demonstrated a nonmonotonic behavior of the θ exponent as the stress increases from the quench. Here we remark that it is only the exponent θ_0 right after the quench affects the scaling in the low stress limit, independent of the θ exponent at higher stress. Theoretically, it turns out to be challenging to find the upper limit of the plastic strain below which the scaling behavior is valid. As we show numerically below, we indeed find the power-law scaling is valid in a finite interval of strain therefore covering an infinite number of avalanches in the thermodynamic limit [2].

II. DIVERGENCE OF THE HIGH-ORDER SHEAR MODULUS

To be simple, we set $\mu = 1$, and the scaling relation between σ and ϵ now becomes $\sigma \sim \gamma - \sigma^{1/\alpha}$. Using Eq. (5), we get

$$\sigma \sim \gamma - \sigma^{1+\theta_0}, \quad (7)$$

and by taking derivatives, we obtain the scaling of the high-order shear modulus as

$$\frac{d^n\sigma}{d\gamma^n} \sim \sigma^{\theta_0+1-n}, \quad (8)$$

with $n \geqslant 2$. Because $0 < \theta_0 < 1$, the high-order shear modulus diverges in the low stress limit. Molecular dynamics simulations indeed have shown that the nonlinear elasticity

$\sigma = \mu\gamma + \mu_2\gamma^2 + \mu_3\gamma^3 + \cdots$ breaks down for amorphous solids [4,27–29]. A finite θ exponent in the distribution of local stabilities not only affects the distribution of avalanches [2,30], but also has a strong impact on the stress-strain curve. Our theories are consistent with recent calculations in the infinite dimension [1], which shows the divergence of the high-order shear modulus at low temperatures. In the following, we test our results using two very different numerical simulations. Despite the dramatic difference in detail, the scaling relation we obtain between the stress and the plastic strain is universal as we expect.

III. MESOSCOPIC MODEL

We model two- and three-dimensional amorphous solids as consisting of N blocks (sites), each characterized by a scalar local stress σ_i and a local failure threshold σ^{th}. The overall shear stress is $\sigma = \sum_i \sigma_i / N$. We first prepare the system at a finite temperature T with zero shear stress. At zero stress, the sites have an equal chance to yield at the positive and negative thresholds, so the local stability is $x_i = \min(\sigma^{\mathrm{th}} - \sigma_i, \sigma_i + \sigma^{\mathrm{th}})$. We model the effect of finite temperature by the dependence of the local yielding rate on the local stability,

$$r_i = e^{-x_i^2/T} \tag{9}$$

for $x_i > 0$ and $r_i = 1$ for $x_i < 0$. We first let the system equilibrate after a long enough time at temperature T then quench the system to $T = 0$ after which only sites with negative local stabilities can yield. Then we shear the system quasistatically by increasing the shear stress σ until the least stable site yields. Unstable sites have a constant rate of $1/\tau_c$ to yield. A local yielding increases the local plastic strain $\delta\epsilon_i = \epsilon_0$ and an overall increment of plastic strain $\delta\epsilon = \epsilon_0/N$. The local yielding also reduces the stress locally by some amount $\delta\sigma_i = \mu\,\delta\epsilon_i$ where μ is the shear modulus and affects stress in other locations via a long-range Eshelby field $\delta\sigma_j = \mathcal{G}(\vec{r}_{ij})\Delta\sigma_i$ [21], which can in turn trigger new instabilities. We shear the system using the stress-control method and periodic boundary condition, so the shear stress is fixed during avalanches and increases between avalanches. We set $\sigma^{\mathrm{th}} = 0.55$, $\epsilon_0 = \mu = \tau_c = 1$ in both two and three dimensions.

IV. ATOMISTIC SIMULATIONS

We also perform numerical simulations based on real spherical particles. The systems are two or three dimensional with side length L in all directions. To avoid crystallization, we set $N/2$ large and $N/2$ small disks with equal mass m in the system. The diameter ratio of the large to small particles is 1.4. The interparticle potential is

$$U(r_{ij}) = \begin{cases} u(1 - r_{ij}/d_{ij})^2/2 & \text{for } r_{ij} < d_{ij}, \\ 0 & \text{for } r_{ij} \geqslant d_{ij}, \end{cases} \tag{10}$$

where r_{ij} and d_{ij} are the separation between the particles i and j and the sum of their radii. We set the units of mass, energy, and length to be m, u, and a small particle diameter. Before shear, we generate 100 static states at fixed packing fractions $\phi = 0.95$ (two dimensions) and $\phi = 0.75$ (three dimensions) by applying the fast inertial relaxation engine minimization method [31] to minimize the potential energy $U = \sum_{ij} U(r_{ij})$

of initially random configurations where the sum is over all pairs of interacting particles. The shear deformation is realized by applying a small shear strain step $\Delta\gamma$ using Lees-Edwards boundary conditions [32,33]. The simulation proceeds by minimizing the total potential energy U after each affine change in the boundary conditions and particle coordinates. We choose the strain step small enough that our results do not depend on the value of $\Delta\gamma$.

V. NUMERICAL RESULTS

We calculate the plastic strain using Eq. (1) and extract the shear modulus from the initial linear slope of the stress-strain curve. We compute the shear modulus from the elastic part of the stress-strain curve before the first avalanche, based on the assumption that the shear modulus is constant during the shear process. We can relax this condition and define the plastic strain alternatively [4]. As illustrated in the inset of Fig. 1(b), we compute the plastic strain as the accumulation of the plastic strain increments ($\delta\epsilon$) during avalanches,

$$\epsilon = \sum_i \delta\epsilon_i. \tag{11}$$

Similarly we define the plastic stress, which is another quantity characterizing the total plastic deformation, as the accumulation of the plastic stress drops ($\delta\sigma_p$),

$$\sigma_p = \sum_i \delta\sigma_{pi}, \tag{12}$$

where i is the index of avalanches and the summation is over all avalanches below the shear stress σ. In the mesoscopic simulations, because the shear modulus is constant, the two definitions of plastic strain Eqs. (1) and (11) and the plastic stress Eq. (12) are all equivalent. For the atomistic simulations, we compare all three calculations of the plastic strain (stress). The resulting relations for both simulations are shown in Fig. 2. Our prediction of $\sigma \sim \epsilon^{2/3}$ (or $\sigma \sim \sigma_p^{2/3}$ for the plastic stress) is satisfyingly confirmed for all cases.

We further test the scaling relation between α and θ_0 by measuring θ_0 independently. For the mesoscopic model, we measure the distribution of local stabilities x right after the quench directly. For the atomistic simulations, we measure the θ_0 exponent indirectly through the finite size scaling of the minimum strain $\gamma_{\min}$ to trigger the first avalanche. Both simulations are consistent with $\theta_0 \approx 0.5$ as shown in Fig. 3.

VI. DISCUSSION

In this paper, we uncover a universal scaling relation between the stress and the plastic strain in the initial stage of the stress-strain curve. The scaling relation is universal and independent of microscopic details as we confirmed using two entirely different simulations. The shear stress turns out to be singularly dependent on the plastic strain due to the plastic avalanches. The main reason for such a singular behavior is the asymmetrical finite size scaling between the strain to trigger the first avalanche $\gamma_{\min} \sim N^{-1/(1+\theta_0)}$ and the plastic strain generated by the first avalanche $\epsilon \sim 1/N$. Because $\alpha = \frac{1}{1+\theta_0}$ and $0 < \theta_0 < 1$, the second- and higher-order shear moduli all diverge in the low stress limit [1,4,27]. So the
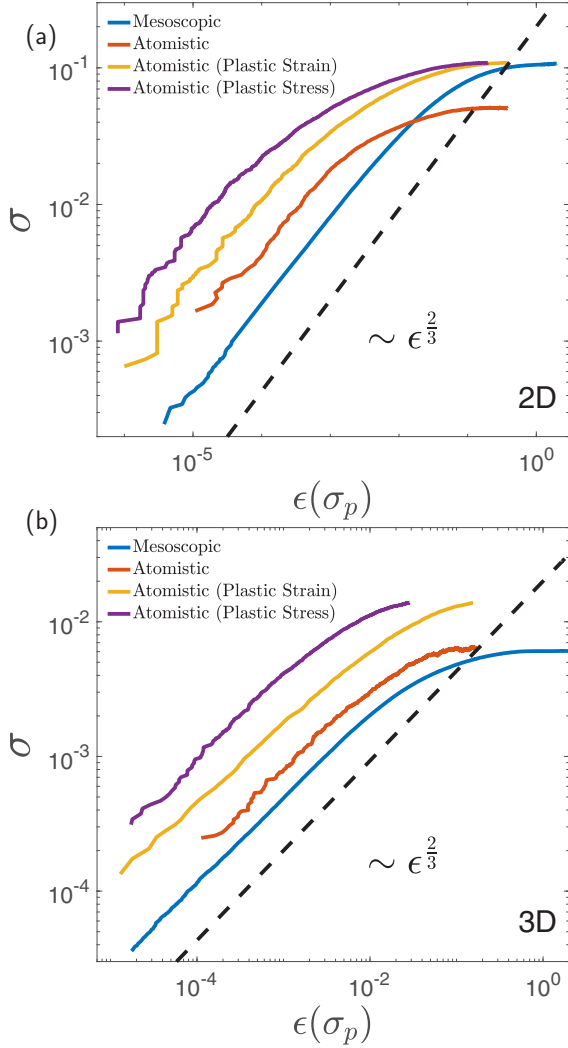
FIG. 2. The stress (σ) vs plastic strain (ϵ) or plastic stress (σ_p) for the mesoscopic simulations and atomistic simulations. The black dashed line has a slope of 2/3. The stress is in arbitrary units. For the mesoscopic simulations, the shear modulus is set to be constant. The system sizes are $N = 512^2$ in 2D and $N = 64^3$ in 3D. The curve is averaged over 100 samples. The initial temperature before the infinite quench is $T = 1$ (2D) and $T = 2$ (3D). For the atomistic simulations, the system sizes are $N = 8192$ (2D) and $N = 4096$ (3D). We first calculate the shear modulus as the average slope of the stress-strain curve in the initial elastic response before the first avalanche. After subtracting the elastic strain according to Eq. (1), we obtain the stress-plastic strain curve for one sample and then average over 100 samples (atomistic). We also compute the plastic strain based on Eq. (11) (plastic strain) and the plastic stress based on Eq. (12) (plastic stress). The curves of the atomistic simulations are shifted arbitrarily on the y axis for clarity. We implement stress-control (strain-control) quasistatic shear to the mescoscopic (atomistic) simulations.

stress-strain curve is far from smooth by nature due to plastic avalanches.

On the experimental side, our paper provides a simple and straightforward method to characterize the plasticity of generic amorphous materials. Given a stress-strain curve, one immediately can obtain the corresponding stress-plastic strain curve by removing the elastic strain. Although the systems we study
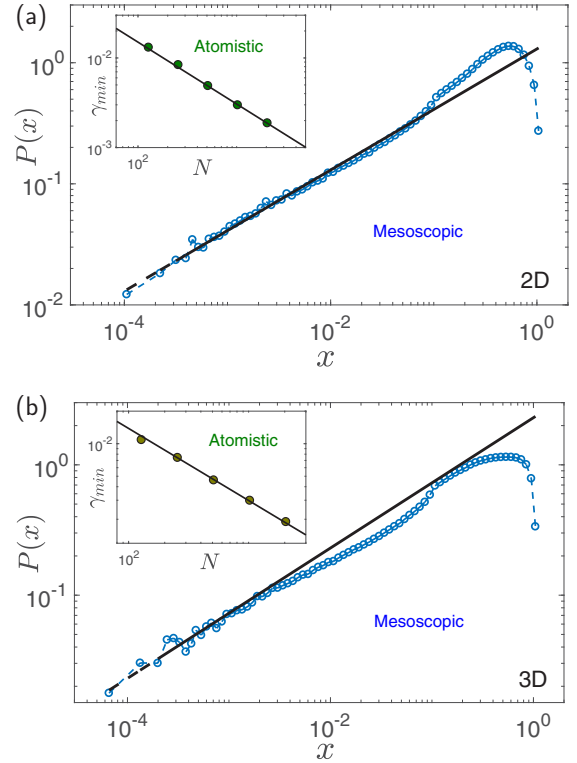

FIG. 3. The distribution of local stabilities $x_i = \sigma^{\text{th}} - \sigma_i$ right after the quench $P(x)$ for the mesoscopic model. The black lines have a slope of 0.5 both for 2D and 3D. The insets: the finite size scaling of the minimum strain to trigger the first avalanche right after a quench for the atomistic simulations. The black lines have a slope of $-2/3$. Using the scaling $\gamma_{\min} \sim N^{-1/(1+\theta_0)}$, we obtain $\theta_0 = 0.5$ as well.

including the coarse-grained model and spherical repulsive particles are idealized, the scaling relation we propose between the shear stress and the plastic strain generally is valid and equally applies to other soft matter systems, e.g., gel, polymer glass, granular material, and colloidal systems [34]. Similar to the Herschel-Bulkley exponent characterizing the flow curves of yield stress materials [7], we uncover a systematic method to identify the universality of plastic deformation. It will be a promising and interesting future direction to unify soft matter systems based on the exponent α we propose.

On the theoretical side, we show that the sublinear scaling between the stress and the plastic strain due to the plastic avalanches is equivalent to the divergence of a high-order shear modulus. Although our theoretical analysis is so simple, we get essentially the same conclusion as other theoretical works based on more involved calculations in the infinite dimensions [1]. Our paper therefore raises a deep question on the connection between these two entirely different approaches, for example, the connection between the pseudogap exponent in the distribution of local stabilities and the so-called Gardner transition [35,36].

It has been shown that decreasing the quench rate could make the system go from ductile to brittle and prone to shear band formation [2,24]. Because the scaling relation between the stress and the plastic strain is for low stress, we expect

the general scaling $\sigma \sim \epsilon^{\alpha}$ is robust against the quench rate. Numerical simulations have reported a larger θ_0 exponent for the slow quench compared with the rapid quench [26], leading to a smaller α. It is certainly a future direction to study the effects of the quench rate on the critical scaling of the stress-strain curve.

[1] G. Biroli and P. Urbani, Nat. Phys. **12**, 1130 (2016).

[2] J. Lin, T. Gueudré, A. Rosso, and M. Wyart, Phys. Rev. Lett. **115**, 168001 (2015).

[3] R. L. Moorcroft and S. M. Fielding, Phys. Rev. Lett. **110**, 086001 (2013).

[4] A. K. Dubey, I. Procaccia, C. A. B. Z. Shor, and M. Singh, Phys. Rev. Lett. **116**, 085502 (2016).

[5] A. Tanguy, F. Leonforte, and J.-L. Barrat, Eur. Phys. J. E **20**, 355 (2006).

[6] A. Lemaître and C. Caroli, Phys. Rev. E **76**, 036104 (2007).

[7] D. Bonn, J. Paredes, M. M. Denn, L. Berthier, T. Divoux, and S. Manneville, Rev. Mod. Phys. **89**, 035005 (2017).

[8] J. Lin, E. Lerner, A. Rosso, and M. Wyart, Proc. Natl. Acad. Sci. USA **111**, 14382 (2014).

[9] K. M. Salerno, C. E. Maloney, and M. O. Robbins, Phys. Rev. Lett. **109**, 105703 (2012).

[10] A. Lemaître and C. Caroli, Phys. Rev. Lett. **103**, 065501 (2009).

[11] K. Martens, L. Bocquet, and J.-L. Barrat, Phys. Rev. Lett. **106**, 156001 (2011).

[12] C. Liu, E. E. Ferrero, F. Puosi, J.-L. Barrat, and K. Martens, Phys. Rev. Lett. **116**, 065501 (2016).

[13] S. Karmakar, E. Lerner, and I. Procaccia, Phys. Rev. E **82**, 055103(R) (2010).

[14] J. Lin, A. Saade, E. Lerner, A. Rosso, and M. Wyart, Europhys. Lett. **105**, 26003 (2014).

[15] H. G. E. Hentschel, P. K. Jaiswal, I. Procaccia, and S. Sastry, Phys. Rev. E **92**, 062302 (2015).

[16] M. L. Falk and J. S. Langer, Phys. Rev. E **57**, 7192 (1998).

[17] A. Amon, V. B. Nguyen, A. Bruand, J. Crassous, and E. Clément, Phys. Rev. Lett. **108**, 135502 (2012).

[18] A. Le Bouil, A. Amon, J.-C. Sangleboeuf, H. Orain, P. Bésuelle, G. Viggiani, P. Chasle, and J. Crassous, Granular Matter **16**, 1 (2014).

[19] C. E. Maloney and A. Lemaître, Phys. Rev. E **74**, 016118 (2006).

[20] J. Lin and M. Wyart, Phys. Rev. X **6**, 011005 (2016).

[21] G. Picard, A. Ajdari, F. Lequeux, and L. Bocquet, Eur. Phys. J. E **15**, 371 (2004).

[22] M. Talamali, V. Petäjä, D. Vandembroucq, and S. Roux, Phys. Rev. E **84**, 016115 (2011).

[23] G. Picard, A. Ajdari, F. Lequeux, and L. Bocquet, Phys. Rev. E **71**, 010501(R) (2005).

[24] M. Fan, M. Wang, K. Zhang, Y. Liu, J. Schroers, M. D. Shattuck, and C. S. O'Hern, Phys. Rev. E **95**, 022611 (2017).

[25] S. Karmakar, E. Lerner, I. Procaccia, and J. Zylberg, Phys. Rev. E **82**, 031301 (2010).

[26] S. Patinet, D. Vandembroucq, and M. L. Falk, Phys. Rev. Lett. **117**, 045501 (2016).

[27] H. G. E. Hentschel, S. Karmakar, E. Lerner, and I. Procaccia, Phys. Rev. E **83**, 061101 (2011).

[28] I. Procaccia, C. Rainone, C. A. B. Z. Shor, and M. Singh, Phys. Rev. E **93**, 063003 (2016).

[29] V. Dailidonis, V. Ilyin, I. Procaccia, and C. A. B. Z. Shor, Phys. Rev. E **95**, 031001(R) (2017).

[30] E. A. Jagla, Phys. Rev. E **92**, 042135 (2015).

[31] E. Bitzek, P. Koskinen, F. Gähler, M. Moseler, and P. Gumbsch, Phys. Rev. Lett. **97**, 170201 (2006).

[32] M. P. Allen and D. J. Tildesley, *Computer Simulation of Liquids* (Oxford University Press, Oxford, 1989).

[33] W. Zheng, H. Liu, and N. Xu, Phys. Rev. E **94**, 062608 (2016).

[34] S. R. Nagel, Rev. Mod. Phys. **89**, 025002 (2017).

[35] P. Charbonneau, J. Kurchan, G. Parisi, P. Urbani, and F. Zamponi, Nat. Commun. **5**, 3725 (2014).

[36] P. Charbonneau, J. Kurchan, G. Parisi, P. Urbani, and F. Zamponi, J. Stat. Mech.: Theory Exp. (2014) P10009.